PD Source Diagnosis and Localization in Industrial High-Voltage Insulation System via Multimodal Joint Sparse Representation

Liangtian Wan, *Member, IEEE*, Guangjie Han, *Member, IEEE*, Lei Shu, *Member, IEEE*, Sammy Chan, *Member, IEEE*, and Naixing Feng, *Student Member, IEEE*

***Abstract*—Partial discharge (PD) is the manifestation of insulation degradation, and it is regarded as a great risk in the field of industrial high-voltage insulation system. In this paper, the direction-of-arrival (DOA) estimation algorithm is used for the localization of partial-discharge source. The intersecting point of two rays, which come from two different directions measured by two uniform linear arrays (ULAs), can be regarded as the plane location of partial-discharge source. Fast rise times of partial-discharge pulses result in a wide electromagnetic spectrum, thus this paper focuses on the DOA estimation of wideband signals. The technique of multimodal joint sparse representation (MJSR) has been used to improve the performance of biometrics recognition. Here, we extend it to DOA estimation. The received data are represented by a sparse linear combination of potential steering vectors, while constraining the observations from different frequencies subject to sharing the same sparsity pattern. Based on the simultaneous orthogonal matching pursuit (SOMP) and alternating direction method of multipliers (ADMM), a hard threshold algorithm is proposed for DOA estimation. In order to reduce the computational complexity of hard threshold algorithm, an improved soft threshold DOA estimation algorithm based on the ADMM is proposed as well. The effectiveness of the proposed algorithms is validated by simulations and real tests.**

***Index Terms*—Direction-of-arrival (DOA) estimation, localization algorithm, multimodal joint sparse representation (MJSR), wideband signal.**

Manuscript received August 27, 2015; revised November 9, 2015 and December 13, 2015; accepted January 9, 2016. Date of publication January 22, 2016; date of current version March 8, 2016. This work was supported in part by the Qing Lan Project, in part by the National Natural Science Foundation of China under Grant 61572172, Grant 61307042, and Grant 61401107, in part by the Natural Science Foundation of Jiangsu Province of China under Grant BK20131137, in part by the 2013 Special Fund of Guangdong Higher School Talent Recruitment, in part by the 2013 Top Level Talents Project in Sailing Plan of Guangdong Province, and in part by the 2014 Guangdong Province Outstanding Young Professor Project. *(Corresponding author: Guangjie Han.)*

L. Wan and G. Han are with the Department of Information and Communication Systems, Hohai University, Changzhou 213022, China (e-mail: wanliangtian1@163.com; hanguangjie@gmail.com).

L. Shu is with Guangdong Petrochemical Equipment Fault Diagnosis Key Laboratory, Guangdong University of Petrochemical Technology, Guangdong 525000, China (e-mail: lei.shu@ieee.org).

S. Chan is with the Department of Electronic Engineering, City University of Hong Kong, Kowloon Tong, Hong Kong (e-mail: eeschan@cityu.edu.hk).

N. Feng is with the Institute of Electromagnetics and Acoustics, Xiamen University, Xiamen 361005, China (e-mail: fengnaixing@gmail.com).

Color versions of one or more of the figures in this paper are available online at http://ieeexplore.ieee.org.

Digital Object Identifier 10.1109/TIE.2016.2520905

Nomenclature

$\mathbf{A}$	Matrix.
$\boldsymbol{a}$	Column vector.
$(\cdot)^*$	Conjugate.
$(\cdot)^{\mathrm{H}}$	Conjugate transpose.
$(\cdot)^{\mathrm{T}}$	Transpose.
$\mathbf{I}_M$	$M \times M$ identical matrix.
ADMM	Alternating direction method of multipliers.
ALM	Augmented Lagrangian method.
CSSM	Coherent signal subspace method.
DFT	Discrete Fourier transform.
diag$\{z_1, z_2\}$	Diagonal matrix whose diagonal entries are z_1 and z_2, respectively.
DOA	Direction-of-arrival.
ISSM	Incoherent signal subspace method.
JLZA-DOA	Joint L0 approximation direction-of-arrival.
L1-SVD	L1-singular value decomposition.
MJSR	Multimodal joint sparse representation.
PD	Partial discharge.
RMSE	Root-mean-square error.
RSSI	Received signal strength indicator.
SNR	Signal-to-noise ratio.
SOMP	Simultaneous orthogonal matching pursuit.
TDOA	Time difference of arrival.
TOA	Time of arrival.
ULA	Uniform linear array.
UHF	Ultrahigh frequency.
W-ADMM-H	Wideband alternating direction method of multipliers hard threshold value.
W-ADMM-S	Wideband alternating direction method of multipliers soft threshold value.
W-CMSR	Wideband covariance matrix sparse representation.
W-SOMP	Wideband simultaneous orthogonal matching pursuit.
WSN	Wireless sensor network.

I. Introduction

PARTIAL discharge (PD) can lead to a great risk in the dielectric stability of an insulation system, and it is the manifestation of insulation degradation. A PD is a discharge phenomenon within an insulation structure defect, such as an air gap, oil film, and a conductor edge, at a certain voltage without

overall insulation breakdown [1]. Confirming the localization of PD source is one of the main methods to diagnose and assess the condition of high-voltage insulation system [2] in modern industry [3].

UHF method has been extensively applied in substations worldwide with excellent results both during high-voltage on-site commissioning tests and condition monitoring during service [4], since it has the advantages of strong anti-interference, high sensitivity, and stable propagation velocity. Many researchers have studied the application of UHF to the field of PD localization and fault diagnosis [1], [5]. Based on the advances in ultrahigh-speed sampling equipment, it is possible to accurately measure the propagation of the PD wavefront as it passes through a four-element antenna array. Then, the arrival time difference was applied to wideband radio-frequency interference of PD sources [5]. The wideband radio-frequency interference generated by PD sources can be used for noninvasive monitoring of discharges. Then, a PD early warning system can be constructed based on radio frequency. The significant advantage of this method lies in the ability to detect PD sources in energized equipment anywhere within a substation compound during normal operating conditions [6]. Accurate position estimations of PD sources depend on the accuracy of arrival time difference [5], [6]. However, accurate estimation of this would be very difficult. Based on three antennas, the noncontact PD measurement using wideband radiometry was adopted to detect the radiated electromagnetic waves generated by PD sources [7]. The angle of arrival estimation is achieved according to the phase difference of different antennas, then the position of PD source was estimated [8]. By the time-of-flight technique, the time difference between wavefronts arriving at two UHF-PD-sensors indicates the location of PD source. Then this technique is transformed into frequency domain, and a high estimation accuracy of PD source is achieved. However, the disadvantage is that the interesting frequency range of the cross correlation and minimum method must be determined manually [9].

PDs in transformers cause multiple resonances in the transformer tank. Fast rise times of PD pulses result in a wide electromagnetic spectrum enabling certain resonances [5], [6], [8], [9]. The recent research about localization of PD sources is based on the array signal processing to achieve a high estimation accuracy [1]. However, its localization algorithm is based on the DOA estimation of narrow signals. This is unreasonable for the real condition for the signals sent by PD sources, since they are all wideband signals. Thus, the DOA estimation algorithms of wideband signals should be used for PD sources' localization. Then, the intersecting point of two rays representing two directions is the location of PD source.

For the DOA estimation of wideband signals, the classic algorithms are ISSM [10] and CSSM [11]. Most of those related methods decompose incident wideband signals into narrowband components, and then realize wideband DOA estimation with incoherent or coherent techniques. The coherent spectral focusing-based methods have been demonstrated to surpass their incoherent counterparts [11], thus these methods have attracted more researchers' interests. However, DOA pre-estimates of incident signals are required for spectral focusing, and the precision of those pre-estimates largely influences the performance of DOA estimation [12]. Recently, based on sparse representation theory, L1-SVD method is proposed in [13], which reduces the dimension of observations via SVD. Convex approximation is introduced and L1-norm is used to facilitate the optimization process [14]. A method called JLZA-DOA was proposed in [15], but the global convergence is not guaranteed. Then, W-CMSR method is proposed in [16]. However, only noncoherent signals can be estimated. In addition, the WSN can be used for source localization as well [17]–[22].

In 2014, MJSR has been proposed in the field of biometrics recognition, which is robustness to noise [23]. Then, a new joint sparse representation model for robust feature-level fusion has been proposed. By using the advantages of sparse representation, unreliable features to be fused for visual tracking can be dynamically removed [24]. Based on task-driven formulation, the multimodal dictionaries have been learned simultaneously with their corresponding image classifiers [25].

Based on MJSR, in this paper, we extend this technique into DOA estimation of wideband signals. First, we construct a large steering matrix containing all the potential directions of all frequency points. Based on SOMP algorithm, the DOAs of wideband signals can be estimated. Second, we propose two ADMM-like algorithms, the DOAs are estimated based on hard and soft threshold value algorithms, respectively. Compared with the algorithm proposed in [1], three algorithms proposed in this paper have much higher estimation accuracy. By solving the intersection of two rays coming from two different DOAs, i.e., two linear equations, the plane coordinates of PD source can be obtained finally. The real data of UHF signals collected in the microwave anechoic chamber prove to be suitable to locate PD sources effectively by the proposed algorithm as well. The accuracy and feasibility of the proposed algorithms are therefore proved.

This paper is organized as follows. The problem formulation of wideband signals is introduced in Section II. The wide SOMP algorithm is proposed in Section II as well. Two ADMM-like algorithms are proposed in Section III. The computational complexity of three algorithms is discussed in Section IV. The improved localization algorithm is introduced in Section V. Simulation results and real test are shown and analyzed in Section VI. Conclusion is drawn in Section VII.

II. DOA Estimation of Wideband Signals

A. Problem Formulation

In a PD detection and localization system, a ULA is used for receiving UHF signals radiated by PD sources. Suppose that K wideband signals with bandwidth B impinge onto a ULA with M sensors from directions of $\theta_1, \ldots, \theta_K$, respectively. The received data of the mth sensor are expressed as

$$x_m(t) = \sum_{k=1}^{K} s_k(t - \tau_{mk}) + n_m(t) \tag{1}$$

where $\tau_{mk}=(m-1)d\sin\theta_k/c$ is the time delay of the kth signal between the mth sensor and the first sensor (it is set as the reference sensor), $s_k(t)$ is the signal complex envelope of the kth signal, and $n_m(t)$ is the additive noise of the mth sensor.

The observation time T_0 is divided into N time intervals, and the duration of each time interval is T_d. Then, J points DFT is taken on the observation data, the received data model of the wideband signals can be expressed as

$$\bar{\mathbf{X}}_n(f_j) = \mathbf{A}(f_j)\,\bar{\mathbf{S}}_n(f_j) + \bar{\mathbf{N}}_n(f_j) \tag{2}$$

where $\bar{\mathbf{X}}_n(f_j)$, $\bar{\mathbf{S}}_n(f_j)$, and $\bar{\mathbf{N}}_n(f_j)$ are the DFT of the received data, signals, and noise, respectively, corresponding to the certain frequency f_j, $n = 1, \ldots, N$, $j = 1, \ldots, J$. The manifold matrix is expressed as

$$\mathbf{A}(f_j) = [\mathbf{a}_1(f_j), \ldots, \mathbf{a}_K(f_j)] \tag{3}$$

where the steering vector is given by

$$\boldsymbol{a}_{jk} = \left[e^{-j2\pi f \tau_{1k}}, \ldots, e^{-j2\pi f \tau_{Mk}}\right]^T. \tag{4}$$

It should be noted that wideband signals with bandwidth B is divided into J sub-bands in frequency domain, which means that there are J equations corresponding to frequencies $f_1, \ldots, f_J$. The problem is stated as follows. We have the frequency data (2) after DFT, then DOAs $\theta_1, \ldots, \theta_K$ are needed to be estimated.

B. DOA Estimation in Sparse Spatial Domain

The DOA estimation problem can be formulated as a sparse representation problem

$$\mathbf{X}^j = \mathbf{\Phi}^j \mathbf{S}^j + \mathbf{N}^j, \quad j = 1, \ldots, J \tag{5}$$

where $\mathbf{X}^j = \left[\bar{\mathbf{X}}_1^j, \ldots, \bar{\mathbf{X}}_N^j\right]$, $\mathbf{\Phi}^j = \left[\mathbf{a}_1^j, \ldots, \mathbf{a}_{\bar{K}}^j\right]$ is an overcomplete steering matrix, $\boldsymbol{a}_i^j$ corresponds to the steering vector of the angle $\bar{\theta}_i$, the set $\mathbf{\Theta} = \left\{\bar{\theta}_1, \ldots, \bar{\theta}_{\bar{K}}\right\}$ is a sampling grid of all potential directions in spatial domain, and $\mathbf{S}^j = \left[\bar{\mathbf{S}}_1^j, \ldots, \bar{\mathbf{S}}_N^j\right]$, $\bar{\boldsymbol{S}}_n^j$ is a sparse vector. The ith element of it is nonzero, if signal k comes from $\bar{\theta}_i$ for some k and zero otherwise, and $\mathbf{N}^j = \left[\bar{\mathbf{N}}_1^j, \ldots, \bar{\mathbf{N}}_N^j\right]$. Thus, $\mathbf{S}^j$ is a sparse matrix with only K nonzero rows associated with actual directions. In general, $\bar{K} \gg M > K$. Note that $\mathbf{\Phi}^j$ is known and it does not depend on the direction of actual signals. It means that the direction of actual signals can be estimated as long as the positions of nonzero values in $\bar{\boldsymbol{S}}_n^j$ are found. $\mathbf{\Phi}^i \neq \mathbf{\Phi}^j, i, j = 1, \ldots, J$, which means the overcomplete steering matrices belonging to different frequencies are different from each other. However, unlike $\mathbf{\Phi}^i$, $\mathbf{S}^i$ has the same sparsity pattern as $\mathbf{S}^j$, i.e., positions of nonzero rows of $\mathbf{S}^i$ are the same as those of $\mathbf{S}^i$.

In more general case, we have J frequency points (modalities). If we denote $\left\{\mathbf{X}^j\right\}_{j=1}^J$ as a set of J observations, and each modality consists of N snapshots. Let $\mathbf{S} = \left[\mathbf{S}^1, \ldots, \mathbf{S}^J\right] \in \mathbb{C}^{\bar{K} \times NJ}$ be the matrix formed by concatenating the potential signal matrices. Then, we can determine the row-sparse matrix $\mathbf{S}$ by solving the following problem:

$$\begin{aligned} &\min_{\mathbf{S}^j} \left\|\mathbf{X}^j - \mathbf{\Phi}^j \mathbf{S}^j\right\|_F^2, j = 1, \ldots, J \\ &\text{s.t. } \|\mathbf{S}\|_{\text{row},0} \leq K \end{aligned} \tag{6}$$

Algorithm 1. W-SOMP algorithm

1: Initialize the residual matrix $\mathbf{R}_0 = \text{diag}\left\{\mathbf{X}^1, \ldots, \mathbf{X}^J\right\}$;
2: the index set $\Lambda_0 = \emptyset$;
3: the iteration counter $t = 1$;
4: **while** not converged **do**
5: update residual matrix $\mathbf{R}_t$;
6: update approximation matrix $\mathbf{A}_t$;
7: update set Λ_t containing t indices, where t is the number of iterations;
8: **end while**;
return residual matrix $\mathbf{R}_T$;
return approximation matrix $\mathbf{A}_T$;
return set Λ_T containing T indices, where T is the number of iterations completed.

where the operator $\|\|_F$ stands for the Frobenius norm of a matrix. In order to solve this problem, we transform (6) into a compact form

$$\begin{aligned} &\min_{\mathbf{\Gamma}} \left\|\text{diag}\left\{\mathbf{X}^1, \ldots, \mathbf{X}^J\right\} - \text{diag}\left\{\mathbf{\Phi}^1, \ldots, \mathbf{\Phi}^J\right\}\mathbf{\Gamma}\right\|_F^2 \\ &\text{s.t. } \|\mathbf{\Gamma}\|_{\text{row},0} \leq K \end{aligned} \tag{7}$$

where $\mathbf{\Gamma} = \left[\mathbf{S}^1, \ldots, \mathbf{S}^J\right]^T \in \mathbb{C}^{J\bar{K} \times N}$. This optimization problem can be solved based on SOMP, which is one of the most simplest greedy methods. However, it should be noted that the dimension of $\text{diag}\left\{\mathbf{\Phi}^1, \ldots, \mathbf{\Phi}^J\right\}$ is tremendous $(MJ \times \bar{K}J)$, which would lead to a huge computational burden for "big data" [26], [27]. The W-SOMP is summarized as follows.

Then, approximation matrix $\mathbf{A}_T$ is the solution of $\mathbf{\Gamma}$, which contains the direction information of incident signals. We divide $\mathbf{A}_T$ into J block matrices with the same form as $\mathbf{\Gamma}$. The final DOA estimation is the nonzero rows of

$$\mathbf{S}_{\text{ave}} = \frac{1}{J}\sum_{j=1}^{J} \mathbf{A}_T^j. \tag{8}$$

III. DOA Estimation Based on ADMM

The optimization problem (6) holds at multiple frequency points, which can be regarded as multimodal multivariate sparse representation problem. This is a convex optimization problem. However, it is difficult to solve due to the joint sparsity constraint. In this section, based on ADMM, we propose an approach to solve (6) based on MJSR. Let

$$C(\mathbf{S}) = \frac{1}{2}\sum_{j=1}^{J} \left\|\mathbf{X}^j - \mathbf{\Phi}^j \mathbf{S}^j\right\|_F^2. \tag{9}$$

Then, (6) is transformed into

$$\min_{\mathbf{S}} C(\mathbf{S}) + \lambda \|\mathbf{S}\|_{\text{row},0} \tag{10}$$

where λ is a positive parameter. The core idea of ADMM is to decouple $C(\mathbf{S})$ and $\|\mathbf{S}\|_{\text{row},0}$ by introducing auxiliary variables

Algorithm 2. ADMM algorithm

1: Initialize $\mathbf{S}_0$, $\mathbf{Z}_0$, $\mathbf{A}_{Z,0}$;
2: **while** not converged **do**
3: $\quad \mathbf{S}_{t+1} = \arg\min_{\mathbf{S}} f_\rho\left(\mathbf{S}, \mathbf{Z}_t, \mathbf{A}_{Z,t}\right)$;
4: $\quad \mathbf{Z}_{t+1} = \arg\min_{\mathbf{Z}} f_\rho\left(\mathbf{S_t}, \mathbf{Z}, \mathbf{A}_{Z,t}\right)$;
5: $\quad \mathbf{A}_{Z,t+1} \doteq \mathbf{A}_{Z,t} + \rho\left(\mathbf{Z}_{t+1} - \mathbf{S}_{t+1}\right)$
6: **end while**.

to reformulate the problem into a constrained optimization problem

$$\begin{aligned} &\min_{\mathbf{S},\mathbf{Z}} C(\mathbf{S}) + \lambda \left\|\mathbf{Z}\right\|_{\text{row},0} \\ &\text{s.t. } \mathbf{Z} = \mathbf{S}. \end{aligned} \tag{11}$$

Since (11) is an equally constrained problem, the ALM can be used to solve it. The augmented Lagrangian function $f_\rho(\mathbf{S}, \mathbf{Z}; \mathbf{A}_Z)$ is defined as

$$C(\mathbf{S}) + \lambda \left\|\mathbf{S}\right\|_{\text{row},0} + \left\langle \mathbf{A}_Z, \mathbf{Z} - \mathbf{S} \right\rangle + \frac{\rho}{2}\left\|\mathbf{Z} - \mathbf{S}\right\|_F^2 \tag{12}$$

where $\mathbf{A}_Z$ is the multiplier of the linear constraint, and ρ is the positive penalty parameter. The ALM algorithm solves $f_\rho(\mathbf{S}, \mathbf{Z}; \mathbf{A}_Z)$ with respect to $\mathbf{S}$ and $\mathbf{Z}$ jointly, keeping $\mathbf{A}_Z$ fixed and then update $\mathbf{A}_Z$ keeping the remaining variables fixed. Due to the separable structure of the objective function f_ρ, one can further simplify the problem by minimizing f_ρ with respect to variables $\mathbf{S}$ and $\mathbf{Z}$, separately. The steps of ADMM are given in Algorithm 2. In what follows, we describe each of the suboptimization problems in detail.

A. Hard Threshold Value Algorithm

1) Update Step for $\mathbf{Z}$*:* The first suboptimization problem involves the minimization $f_\rho\left(\mathbf{S}, \mathbf{Z}; \mathbf{A}_Z\right)$ with respect to $\mathbf{Z}$. Based on the quadratic structure of (12), this minimization can be easily achieved by setting the first-order derivative to zero. Furthermore, the loss function $C(\mathbf{S})$ is a sum of convex functions associated with submatrices $\mathbf{S}^j$, $j = 1, \ldots, J$. Thus, the suboptimization problem is formulated as follows:

$$C\left(\mathbf{S}^j\right) + \lambda \left\|\mathbf{S}\right\|_{\text{row},0} + \left\langle \mathbf{A}_Z^j, \mathbf{Z}^j - \mathbf{S}^j \right\rangle + \frac{\rho}{2}\left\|\mathbf{Z}^j - \mathbf{S}^j\right\|_F^2. \tag{13}$$

Based on the simple method of completing the square, (13) is rewritten as

$$C\left(\mathbf{S}^j\right) + \lambda \left\|\mathbf{S}\right\|_{\text{row},0} + \frac{\rho}{2}\left\|\mathbf{Z}^j - \mathbf{S}^j + \frac{\mathbf{A}_Z^j}{\rho}\right\|_F^2 - \frac{\left\|\mathbf{A}_Z^j\right\|_F^2}{2\rho}. \tag{14}$$

By setting the first-order derivative equal to zero, we have

$$\begin{aligned} \frac{\partial f_\rho\left(\mathbf{S}^j, \mathbf{Z}^j; \mathbf{A}_Z^j\right)}{\partial \mathbf{Z}^j} &= \mathbf{\Phi}^{j^T}\left(\mathbf{X}^j - \mathbf{\Phi}^j \mathbf{Z}^j\right) \\ &\quad + \rho\left(\mathbf{Z}^j - \mathbf{S}^j + \frac{\mathbf{A}_Z^j}{\rho}\right) = 0. \end{aligned} \tag{15}$$

Algorithm 3. W-ADMM-H algorithm

1: Initialize $\mathbf{S}_0$, $\mathbf{Z}_0$, $\mathbf{A}_{Z,0}$;
2: **while** not converged **do**
3: $\quad \mathbf{S}_{t+1} = \left\|\mathbf{Z}_t + \frac{\mathbf{A}_{Z,t}}{\rho}\right\|_{\text{row},0}$;
4: $\quad \mathbf{Z}_{t+1}^j = \left(\mathbf{\Phi}^{j^H}\mathbf{\Phi}^j + \rho\mathbf{I}\right)^{-1} \times \left(\mathbf{\Phi}^{j^H}\mathbf{X}^j + \rho\mathbf{S}_{t+1}^j - \mathbf{A}_{Z,t}^j\right)$;
5: $\quad \mathbf{A}_{Z,t+1} \doteq \mathbf{A}_{Z,t} + \rho\left(\mathbf{Z}_{t+1} - \mathbf{S}_{t+1}\right)$.
6: **end while**.

Then, one seek for the $\mathbf{Z}_{t+1}^j, j = 1, \ldots, J$, which has the following solution:

$$\mathbf{Z}_{t+1}^j = \left(\mathbf{\Phi}^{j^H}\mathbf{\Phi}^j + \rho\mathbf{I}\right)^{-1} \times \left(\mathbf{\Phi}^{j^H}\mathbf{X}^j + \rho\mathbf{S}_t^j - \mathbf{A}_{Z,t}^j\right) \tag{16}$$

where $\mathbf{I}$ is a $\bar{K} \times \bar{K}$ identical matrix, and $\mathbf{S}_t^j$ and $\mathbf{A}_{Z,t}^j$ are the submatrices of $\mathbf{S}_j$ and $\mathbf{A}_Z^j$, respectively.

2) Update Step for $\mathbf{S}$*:* The second suboptimization problem involves the minimization $f_\rho\left(\mathbf{S}, \mathbf{Z}; \mathbf{A}_Z\right)$ with respect to $\mathbf{S}$. The problem can be rewritten as

$$\begin{aligned} &\min_{\mathbf{S}} \frac{\rho}{2}\left\|\mathbf{Z} - \mathbf{S} + \frac{\mathbf{A}_Z}{\rho}\right\|_F^2 \\ &\text{s.t. } \left\|\mathbf{S}\right\|_{\text{row},0} \le K. \end{aligned} \tag{17}$$

Then, $\mathbf{S}$ can be expressed as

$$\mathbf{S}_{t+1} = \left\|\mathbf{Z}_t + \frac{\mathbf{A}_{Z,t}}{\rho}\right\|_{\text{row},0}. \tag{18}$$

This equation means that we calculate the l_2-norm of each row of $\left\|\mathbf{Z} + \frac{\mathbf{A}_Z}{\rho}\right\|_{\text{row},0}$. Based on the values of l_2-norm, we sort the values from large to small, the rows corresponding to the largest K values are chosen and the remaining values of rows are set to zero. This method can be regarded as the hard threshold value algorithm. Thus, the W-ADMM-H algorithm is summarized as follows.

B. Soft Threshold Value Algorithm

According to the equivalence of l_0 and l_1 norm, the optimization problem (6) can be formulated as

$$\min_{\mathbf{S}} C\left(\mathbf{S}^j\right) + \lambda \left\|\mathbf{S}\right\|_{1,q} \tag{19}$$

where q is set to be greater than 1 to make the optimization problem convex. The l_1/l_q regularization seeks a solution with sparse nonzero rows. Hence, we get a representation consistent across all the modalities. The update form of $\mathbf{Z}$ is the same as (16) of the W-ADMM-H algorithm. However, the update of $\mathbf{S}$ has another form.

This suboptimization problem is with respect to $\mathbf{S}$, and it can be reformulated as

$$\min_{\mathbf{S}} \frac{1}{2}\left\|\mathbf{Z}_{t+1} - \mathbf{S} + \frac{\mathbf{A}_{Z,t}}{\rho}\right\|_F^2 + \frac{\lambda}{\rho}\left\|\mathbf{S}\right\|_{1,q}. \tag{20}$$

Due to the separable characteristic of l_1 norm, (20) has the separable structure, it can be solved by minimizing with respect to each row of $\mathbf{S}$ separately. Let $\mathbf{z}_{i,t+1}$, $\mathbf{a}_{i,Z,t}$, and $\mathbf{s}_{i,t+1}$ be the row of $\mathbf{Z}_{t+1}$, $\mathbf{A}_{Z,t}$, and $\mathbf{S}_{t+1}$, respectively. Then, for each $i = 1, \ldots, \bar{K}$, we solve the following subproblem:

$$\mathbf{s}_{i,t+1} = \arg\min_{\mathbf{s}} \frac{1}{2} \|\mathbf{z} - \mathbf{s}\|_F^2 + \eta \|\mathbf{s}\|_q \tag{21}$$

where $\mathbf{z} = \mathbf{z}_{i,t+1} + \mathbf{a}_{i,Z,t}\rho^{-1}$ and $\eta = \frac{\lambda}{\rho}$. One can derive the solution for (21) for any q. In this paper, we only focus on the case with $q = 2$. We have

$$\begin{aligned} \mathbf{s}_{i,t+1} &= \arg\min_{\mathbf{s}} \frac{1}{2} \|\mathbf{z} - \mathbf{s}\|_F^2 + \eta \|\mathbf{s}\|_2 \\ &= \arg\min_{\mathbf{s}} \frac{1}{2} \|\mathbf{z} - \mathbf{s}\|_F^2 + \eta \left(\mathbf{s}^T \mathbf{s}\right)^{1/2}. \end{aligned} \tag{22}$$

This minimization can be easily achieved by setting the first-order derivative equal to zero

$$\begin{aligned} \frac{\partial f}{\partial \mathbf{s}} &= \mathbf{z} - \mathbf{s} + \eta \times \frac{1}{2} \left(\mathbf{s}^T \mathbf{s}\right)^{1/2} \times 2\mathbf{s} \\ &= \mathbf{z} - \mathbf{s} + \eta \frac{\mathbf{s}}{\|\mathbf{s}\|_2} = 0. \end{aligned} \tag{23}$$

Then, $\mathbf{z}$ can be expressed as

$$\mathbf{z} = \left(1 + \frac{\eta}{\|\mathbf{s}\|_2}\right) \mathbf{s}. \tag{24}$$

Letting $\|\mathbf{s}\|_2 = \mathrm{c}, \mathrm{c} > 0$, (24) can be rewritten as

$$\mathbf{z} = \left(1 + \frac{\eta}{c}\right) \mathbf{s}. \tag{25}$$

Equation (25) can be transformed into another form by making the l_2 norm on both sides of (25)

$$\left(1 + \frac{\eta}{c}\right) c = \|\mathbf{z}\|_2. \tag{26}$$

Then, c can be written as

$$c = \|\mathbf{z}\|_2 - \eta > 0. \tag{27}$$

Substituting (27) into (25), we have

$$\mathbf{z} = \left(1 + \frac{\eta}{\|\mathbf{z}\|_2 - \eta}\right) \mathbf{s}. \tag{28}$$

Then, $\mathbf{s}$ can be written as

$$\begin{aligned} \mathbf{s}_{i,t+1} &= \left(1 + \frac{\eta}{\|\mathbf{z}\|_2 - \eta}\right)_+^{-1} \mathbf{z} \\ &= \left(1 - \frac{\eta}{\|\mathbf{z}\|_2}\right)_+ \mathbf{z} \end{aligned} \tag{29}$$

where $(\boldsymbol{c})_+$ is a vector with entries receiving values $\max(\mathbf{c}_i, 0)$. This method can be regarded as the soft threshold value algorithm. Thus, the W-ADMM-S algorithm is summarized as follows.

Algorithm 4. W-ADMM-S algorithm

1: Initialize $\mathbf{S}_0$, $\mathbf{Z}_0$, $\mathbf{A}_{Z,0}$;
2: **while** not converged **do**
3: for each $i = 1, \ldots, \bar{K}$, $\mathbf{s}_{i,t+1} = \left(1 - \frac{\eta}{\|\mathbf{z}\|_2}\right)_+ \mathbf{z}$;
4: $\mathbf{Z}_{t+1}^j = \left(\mathbf{\Phi}^{j^T} \mathbf{\Phi}^j + \rho \mathbf{I}\right)^{-1} \times \left(\mathbf{\Phi}^{j^T} \mathbf{X}^j + \rho \mathbf{S}_t^j - \mathbf{A}_{Z,t}^j\right)$;
5: $\mathbf{A}_{Z,t+1} \doteq \mathbf{A}_{Z,t} + \rho\left(\mathbf{Z}_{t+1} - \mathbf{S}_{t+1}\right)$.
6: **end while**.

IV. Computational Complexity

The main steps of W-ADMM-H and W-ADMM-S algorithms are the update steps for $\mathbf{S}$ and $\mathbf{Z}$. For the W-SOMP algorithm, the dimension of steering matrix $\mathrm{diag}\left\{\mathbf{\Phi}^1, \ldots, \mathbf{\Phi}^J\right\}$ is tremendous $\left(MJ \times \bar{K}J\right)$, it would lead to a huge computational burden.

The dimension of steering matrix of W-SOMP is J times of the W-ADMM-H and W-ADMM-S algorithms. It means that the W-ADMM-H and W-ADMM-S algorithms are more computationally efficient. The W-ADMM-H and W-ADMM-S algorithms can process J suboptimization problems in parallel. This would accelerate the calculation of $\mathbf{Z}$. The update steps for $\mathbf{Z}$ are the same for the W-ADMM-H and W-ADMM-S algorithms. They both involve computing $\left(\mathbf{\Phi}^{j^H} \mathbf{\Phi}^j + \rho \mathbf{I}\right)^{-1}$, and two matrix multiplications. The value of $\left(\mathbf{\Phi}^{j^H} \mathbf{\Phi}^j + \rho \mathbf{I}\right)^{-1}$ is constant across iterations and can be precomputed. This process can reduce lots of computational complexity. Matrix multiplication for two matrices of sizes $m \times n$ and $n \times p$ can be done in $O(mnp)$ time.

However, the update steps of $\mathbf{S}$ are different for the W-ADMM-H and W-ADMM-S algorithms. For the W-ADMM-H algorithm, the values of l_2-norm of each row of $\mathbf{S}$ need to be sorted from large to small. Compared with the W-ADMM-S algorithm, this process would cost lots of computational complexity. Thus, among W-SOMP, W-ADMM-H, and W-ADMM-S algorithms, the computational complexity of the W-ADMM-S algorithm is the lowest.

V. PD Source Localization Based on DOA Estimation

Three ULAs are installed in a substation. Assume that the projection of PD source in the plane of ULAs is S'. The reference points of three ULAs are A, B, and C, respectively. Due to the mirror ambiguity, the incident signal may come from two sides of ULA, as illustrated in Fig. 1. The intersecting point of two rays can be regarded as the location of PD source in principle. It can be seen that S'' and S''' are the intersecting points of two rays as well. However, S'' and S''' are not the actual location of PD source. Thus, another ULA is employed to estimate the DOA of incident signal in order to make sure the actual location of PD source. S' is the intersecting point of three rays, which is regarded as the actual location of PD source.

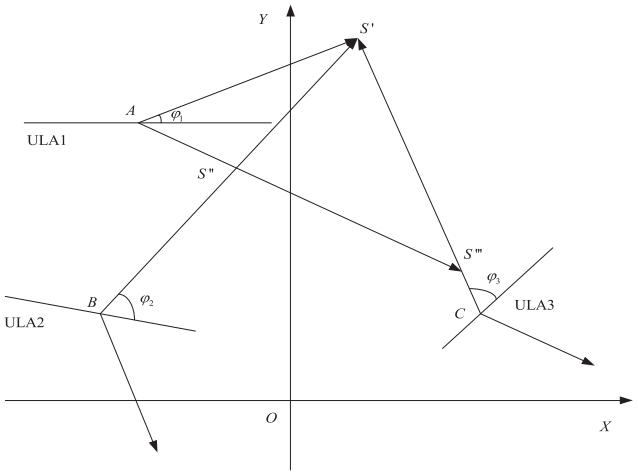

Fig. 1. Position of three ULAs and azimuth of PD source.

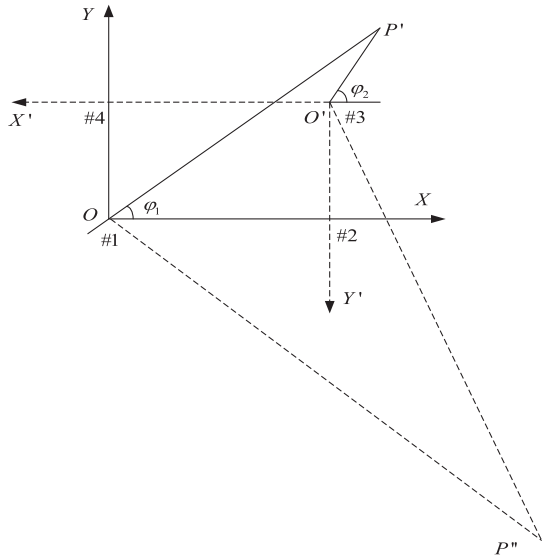

Fig. 2. Planar diagram of sensor array and azimuth of PD source.

Remark 1: In [1], authors give a PD source localization approach, DOA estimation of two L-arrays can be used to localize one PD source. Although an L-array is applied to estimate DOA, the detected range of azimuth is from 0 to π. This means that when the DOAs of incident signals are estimated, the signals may come from both sides of ULA. Fig. 2 in [1] gives the planar diagram of antenna array and azimuth of PD source. We redraw that figure in here as our Fig. 2. The projection of PD source on the sensor array plane is P', the L-shaped array is composed of sensors 1, 2, and 4. A 3-D rectangular coordinate system is established with sensor #1 as the origin as shown in Fig. 2, and the azimuth angle is φ_1. With the same method, consider the L-shaped array formed by sensors #3, #2, and #4 with #3 as the origin, and the azimuth angle is φ_2. The rectangular coordinate system is established according to the dashed lines in Fig. 2. However, another PD source P'' may exist, which is the intersecting point of another two rays. The proposed approach utilizes another ULA to make sure the mirror ambiguity can be avoided.

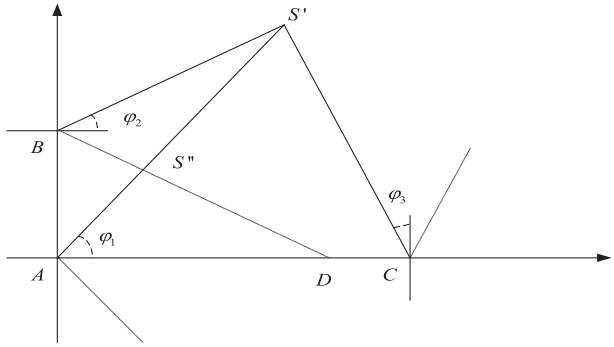

Fig. 3. Position of three ULAs and the actual and fake PD sources.

For the sake of simplicity, an example is shown in Fig. 3. Based on Algorithms 2–4, φ_1, φ_2, and φ_3 can be estimated. The coordinates of reference points A, B, and C corresponding to ULA1, ULA2, and ULA3 are $(0,0)$, $(0,y_B)$, and $(x_C,0)$, respectively. It can be shown that S' is the actual position of PD source, and S'' is a fake one. Based on the measurement of ULA1 and ULA2, we have

$$\tan\varphi_1 = \frac{y}{x} \tag{30}$$

$$\tan\varphi_2 = \frac{y - y_B}{x}. \tag{31}$$

Then, the coordinates of $(x_{S'}, y_{S'})$ can be calculated as

$$x = \frac{y_B}{\tan\varphi_1 - \tan\varphi_2} \tag{32}$$

$$y = \frac{y_B \tan\varphi_1}{\tan\varphi_1 - \tan\varphi_2}. \tag{33}$$

Based on the measurement of ULA1 and ULA3, the coordinates of $(x_{S'}, y_{S'})$ can be calculated as

$$x = \frac{1}{1 + \tan\varphi_1 \tan\varphi_3} x_C \tag{34}$$

$$y = \left(\frac{\tan\varphi_1}{1 + \tan\varphi_1 \tan\varphi_3} x_C\right). \tag{35}$$

If S' is the actual position of PD source, then (32) is equal to (34), and (33) is equal to (35). However, the position of the fake PD source does not satisfy these conditions. The actual position of PD source can thus be decided with three ULAs together.

The RSSI method has been used for localization based on WSNs [28]. However, the attenuation of the signal strength could be changed due to the complex condition of the channel. The estimation accuracy of PD source's location could be severely degraded. TOA [29] is a method that tries to estimate the PD source's position based on the travel time of a signal. However, clock synchronization is one of the challenges involved in the TOA. In [1], a novel algorithm based on DOA estimation is proposed for the localization of PD sources in substations. Planar location of PD sources can be obtained by solving the intersecting point of two lines coming from different DOAs. The time difference in TDOA estimation [30] is replaced by the phase difference in DOA estimation. The benefit of DOA or TDOA compared to TOA is that only the elements' clocks need to be synchronized between each other.

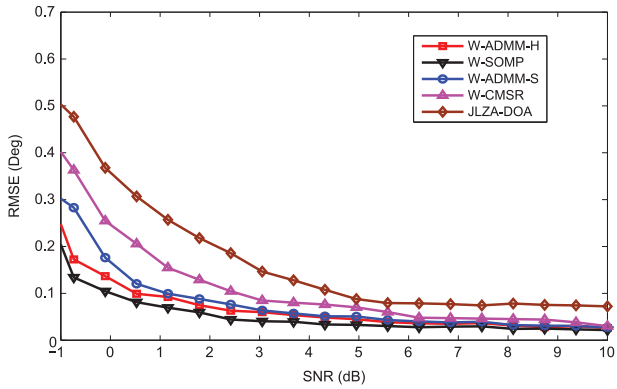

Fig. 4. RMSE versus SNR.

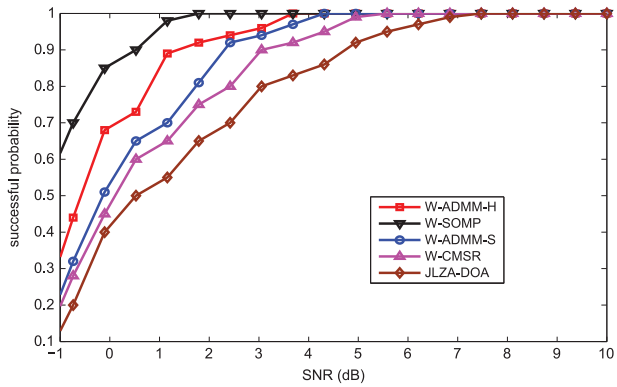

Fig. 5. Successful probability versus SNR.

Compared with RSSI method, the different attenuations of the signal strengths almost do not affect the estimation result of PD source's location. Thus, the application of DOA estimation could be a good choice in the PD source's localization.

VI. Simulation and Real Test Verification

A. Simulation Verification

We compare the performance of the proposed DOA estimation algorithms with JLZA-DOA [15] and W-CMSR algorithms [16] via computer simulation. Assuming that two PD sources impinge on a ULA with eight sensors, and the interspace being is half-wavelength with respect to the highest signal frequency. Two wideband signals come from $44°$ and $68°$, and their frequency spectrum is in the range of 0–1.5 GHz. The received signal is sampled at 4.5 GHz.

We compare the proposed W-SOMP, W-ADMM-H, and W-ADMM-S algorithms with JLZA-DOA and W-CMSR algorithms. The number of independent trials is 100. A trial is regarded as a successful one when the difference between the estimated and true DOA is less than $3°$. The successful probability is counted as the ratio between the number of successful trials and the total number of the independent trials. The RMSE is defined as

$$\mathrm{RMSE} = \sqrt{\frac{1}{N_k}\sum_{k=1}^{N_k}\sum_{i=1}^{q}\left\|\hat{\psi}_i^k - \psi_i\right\|^2} \tag{36}$$

where N_k is the number of independent trials, $\hat{\psi}_i^k$ represents the estimated DOA of the ith signal in the kth trial, and ψ_i represents the true DOA of the ith signal.

First, we test the DOA estimation performance of different algorithms versus SNR. The snapshot number is fixed at 300. The RMSE of different algorithms versus SNR is depicted in Fig. 4. The successful probability of different algorithms versus SNR is depicted in Fig. 5.

It can be seen from Fig. 4 that RMSE becomes smaller as SNR increases for all the algorithms. The correlations as well as coupling information among different frequencies are simultaneously taken into account for the proposed algorithms. Thus, the proposed algorithms outperform the JLZA-DOA and W-CMSR algorithms. For W-SOMP and W-ADMM-H algorithms, they both are applied to solve a l_0 norm minimization problem. For W-SOMP algorithm, the dimension of steering matrix is very large, which contains the information of all the frequency points. The greedy selection strategy is adopted in W-SOMP, which has a higher reconstruction probability than that of W-ADMM-H algorithm. Thus, the RMSE of W-SOMP is smaller than that of W-ADMM-H algorithm. Among the other two algorithms, the RMSE of JLZA-DOA algorithm is larger than that of W-CMSR algorithm. Since there are inherent biases at the points of DOAs in the spectrum of JLZA-DOA. For W-CMSR algorithm, it cannot perform well without the preprocessing of the unified correlation function.

The W-ADMM-S algorithm is applied to solve the l_1 norm minimization problem. Since the l_0 norm minimization problem is NP-hard problem, it cannot be solved in polynomial time. Then, the l_0 norm minimization problem is relaxed to become the l_1 norm minimization problem, which is a convex problem and can be solved in polynomial time. However, this relaxation has a tradeoff, i.e., the solution of l_1 norm minimization is not sparser than that of l_0 norm minimization. Thus, this approximation makes the RMSE of W-ADMM-S larger than that of W-ADMM-H algorithm.

From Fig. 5, it can be seen that when SNR is 5 dB, successful probability of W-SOMP, W-ADMM-H, and W-ADMM-S algorithms approximates to 100%. The successful probability of W-SOMP algorithm is higher than that of other two algorithms in low SNR, which is verified by the results of Fig. 4. It should be noted that the ADMM algorithm does not always converge when it is applied to solve the nonconvex problem (the l_0 norm minimization problem). This is another reason that the successful probability of W-ADMM-H is lower than that of W-SOMP algorithm. Among the other two algorithms, the successful probability of W-CMSR is higher than that of JLZA-DOA algorithm even when the SNR is low. When SNR reaches 5 dB, the successful probability of W-CMSR reaches 100%. However, JLZA-DOA algorithm needs 8 dB. The results of successful probability of JLZA-DOA and W-CMSR algorithms are identical with those of RMSE.

Second, we test the DOA estimation performance of different algorithms versus snapshot number. The SNR is fixed at 3 dB. Other simulation conditions are identical with that of Fig. 4. The RMSE of different algorithms versus snapshot number is depicted in Fig. 6. The successful probability of different algorithms versus snapshot number is depicted in Fig. 7.

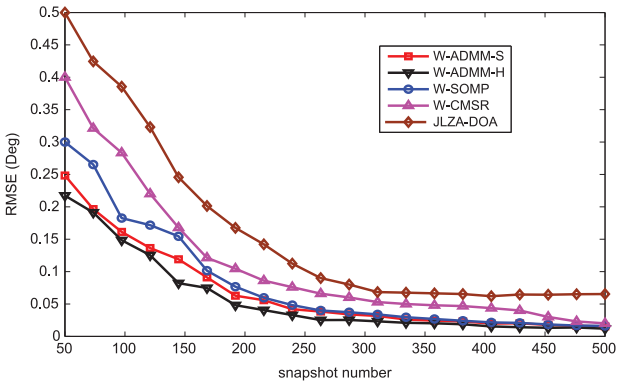

Fig. 6. RMSE versus snapshot number.

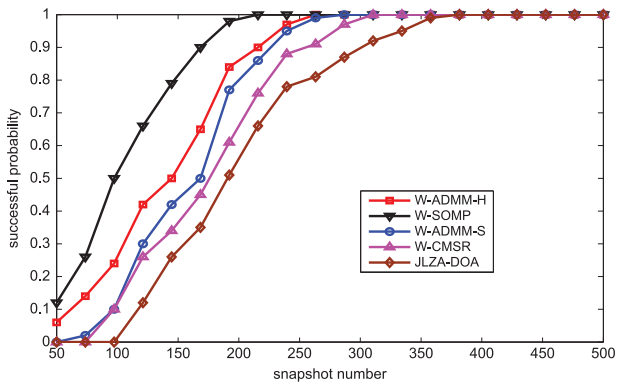

Fig. 7. Successful probability versus snapshot number.

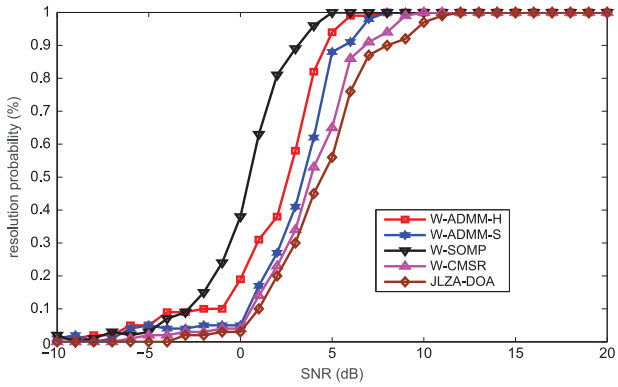

Fig. 8. Resolution probability versus SNR.

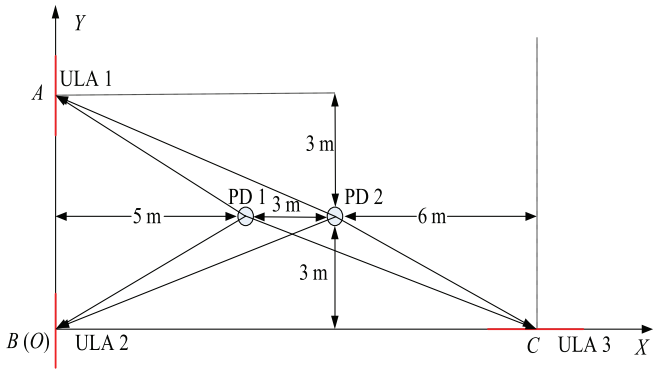

Fig. 9. Planar diagram of three ULAs and two PD sources.

It can be seen from Fig. 6 that RMSE becomes smaller as snapshot number increases for all the algorithms. The proposed W-SOMP and W-ADMM-H algorithms outperform W-ADMM-S algorithm. This is mainly because the solution of l_1 norm minimization is not sparser than that of l_0 norm minimization. Among the other two algorithms, the RMSE of JLZA-DOA algorithm is larger than that of W-CMSR algorithm. When the SNR is larger than 300, the variation of the RMSE is little, since there are inherent biases at the points of DOAs in the spectrum of JLZA-DOA.

For the successful probability shown in Fig. 7, the W-SOMP algorithm outperforms W-ADMM-H and W-ADMM-S algorithms. This result is identical with the first experiment with respect to SNR. Among the other two algorithms, the successful probability of W-CMSR is higher than that of JLZA-DOA algorithm. When the snapshot number reaches 320, the successful probability of W-CMSR approximates to 100%. However, JLZA-DOA algorithm needs 380 snapshot numbers.

Fig. 8 shows the resolution probability versus SNR for the proposed algorithms when the sources are closely spaced (6 degrees separation). The elevation and azimuth of the incident signals are $54°$ and $60°$, respectively. Other simulation conditions are the same as those in the first experiment. The two incident signals are resolved if $|\widehat{\varphi}_1 - \varphi_1|$ and $|\widehat{\varphi}_2 - \varphi_2|$ are smaller than $|\varphi_1 - \varphi_2|/2$. $\widehat{\varphi}_i$ and φ_i represent the estimated and real azimuths for *i*th incident signal, respectively.

Fig. 8 shows that the resolution performance of W-SOMP algorithm outperforms another two algorithms in a relatively low SNR (-2 to 8 dB). When SNR is smaller than -2 dB, the proposed algorithms do not perform well, since the effect of noise is fairly remarkable. It results in the relatively poor resolution performance of the proposed algorithms in low SNR. However, when SNR is larger than 8 dB, the resolution performance of the proposed algorithms reaches 100%. Among the other two algorithms, W-CMSR performs better than JLZA-DOA algorithm. In-depth analysis of the JLZA-DOA spectrum shows that the actual spectrum peaks often fork at the top, which may puzzle the user in judging whether there is one or two adjacent signals. The details can be found in [14]. This phenomenon has blocked JLZA-DOA from obtaining satisfying DOA estimation performance.

Thus, when high accuracy of DOA estimation is required, the W-SOMP algorithm should be selected, and the tradeoff is a large computational burden. When real-time processing is required, the W-ADMM-S algorithm should be selected, and the tradeoff is the relatively low estimation accuracy. The W-ADMM-H algorithm is in the middle for both the estimation accuracy and real-time processing. Then, based on the cross-location method, the location of PD source can be estimated finally.

Finally, we test PD source's localization performance of W-ADMM-H, JLZA-DOA, and W-CMSR algorithms versus SNR. Planar diagram of three ULAs and two PD sources is shown in Fig. 9. The reference coordinates of three UlAs are $A(0, 6, 4)$ m, $B(0, 0, 4)$ m, and $C(14, 0, 4)$ m, respectively. The positions of PD sources are $P_1(5, 3, 1)$ m and $P_2(8, 3, 1)$ m, respectively. Assume that the signals directly reach the receivers.

TABLE I
LOCATION RESULTS AND ERRORS OF PD SOURCE BY W-ADMM-H

SNR (dB)	(x_{p1}, y_{p1}) (m)	Error (cm)	(x_{p1}, y_{p1}) (m)	Error (cm)
20	(4.96, 3.04)	8	(7.96, 2.96)	8
15	(5.08, 3.06)	14	(8.06, 2.94)	12
10	(5.11, 3.08)	19	(8.10, 3.12)	22
5	(5.16, 3.11)	27	(8.14, 3.16)	30

TABLE II
LOCATION RESULTS AND ERRORS OF PD SOURCE BY W-CMSR

SNR (dB)	(x_{p1}, y_{p1}) (m)	Error (cm)	(x_{p1}, y_{p1}) (m)	Error (cm)
20	(4.94, 3.07)	13	(7.98, 2.95)	7
15	(5.12, 3.10)	22	(8.10, 2.96)	14
10	(5.15, 3.12)	27	(8.13, 3.15)	28
5	(5.21, 3.16)	37	(8.18, 3.19)	37

TABLE III
LOCATION RESULTS AND ERRORS OF PD SOURCE BY JLZA-DOA

SNR (dB)	(x_{p1}, y_{p1}) (m)	Error (cm)	(x_{p1}, y_{p1}) (m)	Error (cm)
20	(4.92, 3.10)	18	(7.96, 2.91)	13
15	(5.16, 3.14)	30	(8.15, 3.10)	19
10	(5.20, 3.16)	36	(8.17, 3.19)	36
5	(5.29, 3.19)	48	(8.24, 3.23)	47

TABLE IV
LOCATION RESULTS AND ERRORS OF PD SOURCE BY THE PROPOSED ALGORITHM

SNR (dB)	(x_{p1}, y_{p1}) (m)	Error (cm)	(x_{p1}, y_{p1}) (m)	Error (cm)
20	(5.10, 3.07)	17	(7.90, 2.90)	20
15	(5.15, 3.09)	24	(8.12, 2.90)	22
10	(5.21, 3.12)	33	(8.10, 3.19)	29
5	(5.25, 3.19)	44	(8.17, 3.23)	40

Theoretical values of azimuth angles are $\varphi_A^1 = -30.96°$, $\varphi_B^1 = 30.96°$, $\varphi_C^1 = 71.57°$, and $\varphi_A^2 = -20.56°$, $\varphi_B^2 = 20.56°$, $\varphi_C^2 = 63.43°$. The snapshot number is fixed at 100.

Planar location of the PD sources' locations can be obtained using the mean values of azimuths estimated above by (32) and (33) or (34) and (35). The localization results and their errors based on DOA of different algorithms versus SNR are shown in Tables I–III, respectively. It can be known that the W-ADMM-H performs best, the localization error is the smallest of three algorithms. This result is identical with that of the DOA estimation accuracy.

B. Real Test Verification

In this section, the proposed algorithm is tested in real application. The real test is taken in a microwave anechoic chamber. Its height, width, and length are 18, 10, and 15 m, respectively. The proposed DOA-based localization method is compared with the ESPRIT-based algorithm proposed in [1] and the TOA-based algorithm [29] to verify the effectiveness of the proposed method. The positions of three ULAs and two PD sources are the same as that of the simulation. The planar diagram is shown in Fig. 9. The frequency spectrum of two wideband signals is in the range of 0–1 GHz. The received signal is sampled at 4 GHz. The snapshot number is fixed at 100. The localization results and their errors of different algorithms versus SNR are shown in Tables IV–VI, respectively.

It can be shown that the localization accuracy of ESPRIT-based algorithm is similar to that of TOA-based algorithm.

TABLE V
LOCATION RESULTS AND ERRORS OF PD SOURCE BY ESPRIT

SNR (dB)	(x_{p1}, y_{p1}) (m)	Error (cm)	(x_{p1}, y_{p1}) (m)	Error (cm)
20	(5.12, 3.09)	21	(8.10, 2.94)	16
15	(5.19, 3.11)	30	(8.14, 2.88)	26
10	(5.25, 3.17)	42	(8.16, 3.23)	39
5	(5.29, 3.29)	58	(8.22, 3.29)	51

TABLE VI
LOCATION RESULTS AND ERRORS OF PD SOURCE BY TOA

SNR (dB)	(x_{p1}, y_{p1}) (m)	Error (cm)	(x_{p1}, y_{p1}) (m)	Error (cm)
20	(5.19, 3.14)	33	(8.12, 2.96)	16
15	(5.24, 3.16)	40	(8.19, 2.87)	32
10	(5.29, 3.21)	51	(8.21, 3.21)	42
5	(5.36, 3.25)	61	(8.24, 3.22)	46

Since the ULA is used, ESPRIT-based algorithm is merely used for one-dimensional DOA estimation. The cumulants of the signals cannot be used. This causes the performance degradation of ESPRIT-based algorithm. The proposed localization algorithm can obtain better localization accuracy as compared with others. The superior localization performance of the proposed algorithm is verified by this real test.

VII. CONCLUSION

In this paper, a localization algorithm for PD source in industrial high-voltage insulation system has been proposed based on three ULAs. The position of PD sources can be decided by the intersecting point of two rays sent by two ULAs. Another ULA is applied to eliminate the mirror ambiguity. The localization algorithm is based on estimating DOA of PD sources via MJSR theory. For l_0 norm minimization, two DOA estimation algorithms named W-SOMP and W-ADMM-H algorithms are proposed. For l_1 norm minimization, an algorithm named W-ADMM-S is proposed. Finally, the position of PD source can be located with a high accuracy based on the cross-location method.

REFERENCES

[1] H. Hou, G. Sheng, and X. Jiang, "Localization algorithm for the PD source in substation based on L-shaped antenna array signal processing," *IEEE Trans. Power Del.*, vol. 30, no. 1, pp. 472–479, Feb. 2015.
[2] H. Mirzaei, A. Akbari, E. Gockenbach, and K. Miralikhani, "Advancing new techniques for UHF PD detection and localization in the power transformers in the factory tests," *IEEE Trans. Dielect. Elect. Insul.*, vol. 22, no. 1, pp. 448–455, Feb. 2015.
[3] S. Yin, X. Li, H. Gao, and O. Kaynak, "Data-based techniques focused on modern industry: An overview," *IEEE Trans. Ind. Electron.*, vol. 62, no. 1, pp. 657–667, Jan. 2015.
[4] J. Lopez-Roldan, M. Blundell, T. Irwin, and C. Charlson, "Partial discharge diagnostics for mixed-technology switchgear (MTS) in outdoor substations," *IEEE Power Energy Mag.*, vol. 29, no. 3, pp. 41–47, May/Jun. 2013.
[5] H. Hou, G. Sheng, and X. Jiang, "Robust time delay estimation method for locating UHF signals of partial discharge in substation," *IEEE Trans. Power Del.*, vol. 28, no. 3, pp. 1960–1968, Jul. 2013.
[6] I. E. Portugues, P. J. Moore, I. A. Glover, C. Johnstone, R. H. McKosky, and M. B. Goff, "RF-based partial discharge early warning system for air-insulated substations," *IEEE Trans. Power Del.*, vol. 24, no. 1, pp. 20–28, Jan. 2009.
[7] F. Sacuto, F. Labeau, and B. L. Agba, "Wide band time-correlated model for wireless communications under impulsive noise within power substation," *IEEE Trans. Wireless Commun.*, vol. 13, no. 3, pp. 1449–1461, Mar. 2014.

[8] Y. Tian, A. Tatematsu, K. Tanabe, and K. Miyajima, "Development of locating system of pulsed electromagnetic interference source based on advanced TDOA estimation method," *IEEE Trans. Electromagn. Compat.*, vol. 56, no. 6, pp. 1326–1334, Dec. 2014.

[9] J. Lopez-Roldan, T. Tang, and M. Gaskin, "Optimisation of a sensor for onsite detection of partial discharges in power transformers by the UHF method," *IEEE Trans. Dielect. Elect. Insul.*, vol. 15, no. 6, pp. 1634–1639, Dec. 2008.

[10] J. W. Shin, Y. J. Lee, and H. N. Kim, "Reduced-complexity maximum likelihood direction-of-arrival estimation based on spatial aliasing," *IEEE Trans. Acoust. Speech Signal Process.*, vol. 62, no. 24, pp. 6568–6581, Dec. 2014.

[11] J. Yu, L. Zhang, and K. Liu, "Coherently distributed wideband LFM source localization," *IEEE Signal Process. Lett.*, vol. 22, no. 4, pp. 504–508, Apr. 2015.

[12] L. Wang, L. Zhao, G. Bi, C. Wan, L. Zhang, and H. Zhang, "Novel wideband DOA estimation based on sparse Bayesian learning with Dirichlet process priors," *IEEE Trans. Signal Process.*, vol. 64, no. 2, pp. 275–289, Jan. 2016.

[13] D. Malioutov, M. Cetin, and A. S. Willsky, "A sparse signal reconstruction perspective for source localization with sensor arrays," *IEEE Trans. Signal Process.*, vol. 53, no. 8, pp. 3010–3022, Aug. 2005.

[14] G. Lerman, M. B. McCoy, J. A. Tropp, and T. Zhang, "Robust computation of linear models by convex relaxation," *Found. Comput. Math.*, vol. 15, no. 2, pp. 363–410 Apr. 2015.

[15] M. M. Hyder and K. Mahata, "Direction-of-arrival estimation using a mixed L2,0 norm approximation," *IEEE Trans. Signal Process.*, vol. 58, no. 9, pp. 4646–4655, Sep. 2010.

[16] Z. M. Liu, T. Z. Huang, and Y. Y. Zhou, "Direction-of-arrival estimation of wideband signals via covariance matrix sparse representation," *IEEE Trans. Signal Process.*, vol. 59, no. 9, pp. 4256–4270, Sep. 2011.

[17] Y. Ji, C. Yu, J. Wei, and B. Anderson, "Localization bias reduction in wireless sensor networks," *IEEE Trans. Ind. Electron.*, vol. 62, no. 5, pp. 3004–3016, May 2015.

[18] G. Han, H. Xu, T. Q. Duong, J. Jiang, and T. Hara, "Localization algorithms of wireless sensor networks: A survey," *Telecommun. Syst.*, vol. 52, no. 4, pp. 2419–2436, Apr. 2013.

[19] S. Yin and Z. Huang, "Performance monitoring for vehicle suspension system via fuzzy positivistic C-means clustering based on accelerometer measurements," *IEEE/ASME Trans. Mechatronics*, vol. 20, no. 5, pp. 2613–2620, Oct. 2015.

[20] B. Martinez, X. Vilajosana, F. Chraim, I. Vilajosana, and K. S. J. Pister, "When scavengers meet industrial wireless," *IEEE Trans. Ind. Electron.*, vol. 62, no. 5, pp. 2994–3003, May 2015.

[21] G. Han, J. Chao, C. Zhang, L. Shu, and Q. Li, "The impacts of mobility models on DV-hop based localization in mobile wireless sensor networks," *J. Netw. Comput. Appl.*, vol. 42, no. 6, pp. 70–79, Jun. 2014.

[22] Z. Yang, X. Shi, and J. Chen, "Optimal coordination of mobile sensors for target tracking under additive and multiplicative noises," *IEEE Trans. Ind. Electron.*, vol. 61, no. 7, pp. 3459–3468, Jul. 2014.

[23] S. Shekhar, V. M. Patel, N. M. Nasrabadi, and R. Chellappa, "Joint sparse representation for robust multimodal biometrics recognition," *IEEE Trans. Pattern Anal. Mach. Intell.*, vol. 36, no. 1, pp. 113–126, Jan. 2014.

[24] X. Lan, A. J. Ma, P. C. Yuen, and R. Chellappa, "Joint sparse representation and robust feature-level fusion for multi-cue visual tracking," *IEEE Trans. Image Process.*, vol. 24, no. 12, pp. 5826–5841, Dec. 2015.

[25] S. Bahrampour, N. M. Nasrabadi, A. Ray, and W. K. Jenkins, "Multimodal task-driven dictionary learning for image classification," *IEEE Trans. Image Process.*, vol. 25, no. 1, pp. 24–38, Jan. 2016.

[26] S. Yin and O. Kaynak, "Big data for modern industry: Challenges and trends," *Proc. IEEE*, vol. 102, no. 3, pp. 143–146, Feb. 2015.

[27] Q. Wei and D. Liu, "Data-driven neuro-optimal temperature control of water-gas shift reaction using stable iterative adaptive dynamic programming," *IEEE Trans. Ind. Electron.*, vol. 61, no. 11, pp. 6399–6408, Nov. 2014.

[28] J. P. Beaudeau, M. F. Bugallo, and P. M. Djuric, "RSSI-based multi-target tracking by cooperative agents using fusion of cross-target information," *IEEE Trans. Signal Process.*, vol. 63, no. 19, pp. 5033–5044, Oct. 2015.

[29] H. Shen, Z. Ding, S. Dasgupta, and C. Zhao, "Multiple source localization in wireless sensor networks based on time of arrival measurement," *IEEE Trans. Signal Process.*, vol. 62, no. 8, pp. 1938–1949, Apr. 2014.

[30] B. Huang, L. Xie, and Z. Yang, "TDOA-based source localization with distance-dependent noises," *IEEE Trans. Wireless Commun.*, vol. 14, no. 1, pp. 468–480, Jan. 2015.

Liangtian Wan (M'15) received the B.S. and Ph.D. degrees in information and communication engineering from Harbin Engineering University, Harbin, China, in 2011 and 2015, respectively.

He is currently a Visiting Scholar at Hohai University, Changzhou, China. He has authored over 30 papers published in related international conference proceedings and journals. His research interests include array signal processing and compressed sensing and its applications.

Dr. Wan was a Guest Editor of IEEE ACCESS, and has served as a Reviewer for more than ten journals and Technical Program Committee member of several international conferences.

Guangjie Han (S'03–M'05) received the Ph.D degree in computer science from Northeastern University, Shenyang, China, in 2004.

He was a Postdoctoral Researcher with the Department of Computer Science, Chonnam National University, Gwangju, Korea, in 2008. He is currently a Professor with the Department of Communication and Information System, Hohai University, Changzhou, China. He was also a Visiting Research Scholar at Osaka University, Suita, Japan, from 2010 to 2011. His research interests include security and trust management, localization and tracking, and routing for sensor networks.

Dr. Han has served as an Editor of the *KSII Transactions on Internet and Information Systems* and the *Journal of Internet Technology*.

Lei Shu (M'07) received the Ph.D. degree in computer science from the National University of Ireland, Galway, Ireland, in 2010.

Until March 2012, he was a Specially Assigned Researcher with the Department of Multimedia Engineering, Graduate School of Information Science and Technology, Osaka University, Suita, Japan. Since October 2012, he has been a Full Professor with Guangdong University of Petrochemical Technology, Maoming, China. He is also the Vice-Director of the Guangdong Provincial Key Laboratory of Petrochemical Equipment Fault Diagnosis, Maoming, China. He is the Founder of the Industrial Security and Wireless Sensor Networks Laboratory at Guangdong University of Petrochemical Technology. His research interests include wireless sensor networks, multimedia communication, middleware, security, and fault siagnosis.

Dr. Shu is a member of the European Alliance for Innovation (EAI) and the Association for Computing Machinery (ACM).

Sammy Chan (S'87–M'89) received the B.E. and M.Eng.Sc. degrees in electrical engineering from The University of Melbourne, Melbourne, Australia, in 1988 and 1990, respectively, and the Ph.D. degree in communication engineering from the Royal Melbourne Institute of Technology, Melbourne, Australia, in 1995.

From 1989 to 1994, he was with the Telecom Australia Research Laboratories, Clayton, Australia, first as a Research Engineer, and between 1992 and 1994 as a Senior Research Engineer and Project Leader. Since December 1994, he has been with the Department of Electronic Engineering, City University of Hong Kong, Kowloon Tong, Hong Kong, where he is currently an Associate Professor.

Naixing Feng (S'16) received the B.S. degree in electronic science and technology and the M.S. degree in microelectronics and solid-state electronics from Tianjin Polytechnic University, Tianjin, China, in 2010 and 2013, respectively. He is currently working toward the Ph.D. degree in radio physics at Xiamen University, Xiamen, China, and as a joint Ph.D. student with the Department of Electrical and Computer Engineering, Duke University, Durham, NC, USA.

He has authored over 20 papers published in refereed journals and conference proceedings. His research interests include computational electromagnetics and acoustics.

Dr. Feng has served as a Reviewer of more than five journals.